J. Biochem. 2016;159(5):527–538 doi:10.1093/jb/mvv133

JB THE JOURNAL OF BIOCHEMISTRY

Redox-coupled structural changes in nitrite reductase revealed by serial femtosecond and microfocus crystallography

Received August 11, 2015; accepted November 19, 2015; published online January 14, 2016

Yohta Fukuda[1,*], Ka Man Tse[1,†], Mamoru Suzuki[2,3,†,‡], Kay Diederichs[4,†], Kunio Hirata[3,†], Takanori Nakane[5], Michihiro Sugahara[3], Eriko Nango[3], Kensuke Tono[6], Yasumasa Joti[6], Takashi Kameshima[6], Changyong Song[3,7], Takaki Hatsui[3], Makina Yabashi[3], Osamu Nureki[5], Hiroyoshi Matsumura[1,*], Tsuyoshi Inoue[1,§], So Iwata[3,8] and Eiichi Mizohata[1,¶]

[1]Department of Applied Chemistry, Graduate School of Engineering, Osaka University, 2-1 Yamadaoka, Suita, Osaka 565-0871, Japan; [2]Institute for Protein Research, Osaka University, 3-2 Yamadaoka, Suita, Osaka 565-0871, Japan; [3]RIKEN SPring-8 Center, 1-1-1 Kouto, Sayo-cho, Sayo-gun, Hyogo 679-5148, Japan; [4]Department of Biology, University of Konstanz, D-78457 Konstanz, Germany; [5]Department of Biological Sciences, Graduate School of Science, The University of Tokyo, 7-3-1 Hongo, Bunkyo-ku, Tokyo 113-0033, Japan; [6]Japan Synchrotron Radiation Research Institute, 1-1-1 Kouto, Sayo-cho, Sayo-gun, Hyogo 679-5198, Japan; [7]Department of Physics, Pohang University of Science and Technology, Pohang 790-784, Korea; and [8]Department of Cell Biology, Graduate School of Medicine, Kyoto University, Yoshidakonoe-cho, Sakyo-ku, Kyoto, 606-8501, Japan

*Present addresses: Yohta Fukuda, Department of Biochemistry and Molecular Biophysics, Columbia University, 650 W 168 Street, NY 10032, USA; Hiroyoshi Matsumura, Department of Biotechnology, College of Life Sciences, Ritsumeikan University, 1-1-1 Noji-higashi, Kusatsu Shiga 525-8577, Japan.

†These authors contributed equally to this work.

‡Mamoru Suzuki, Institute for Protein Research, Osaka University, 3-2 Yamadaoka, Suita, Osaka 565-0871, Japan. Tel: +81-6-6879-8637, Fax: +81-6-6879-4313, email: mamoru.suzuki@protein.osaka-u.ac.jp

§Tsuyoshi Inoue, Department of Applied Chemistry, Graduate School of Engineering, Osaka University, 2-1 Yamadaoka, Suita, Osaka 565-0871, Japan. Tel: +81-6-6879-7408, Fax: +81-6-6879-7409, email: inouet@chem.eng.osaka-u.ac.jp

¶Eiichi Mizohata, Department of Applied Chemistry, Graduate School of Engineering, Osaka University, 2-1 Yamadaoka, Suita, Osaka 565-0871, Japan. Tel: +81-6-6879-7410, Fax: +81-6-6879-7409, email: mizohata@chem.eng.osaka-u.ac.jp

Serial femtosecond crystallography (SFX) has enabled the damage-free structural determination of metalloenzymes and filled the gaps of our knowledge between crystallographic and spectroscopic data. Crystallographers, however, scarcely know whether the rising technique provides truly new structural insights into mechanisms of metalloenzymes partly because of limited resolutions. Copper nitrite reductase (CuNiR), which converts nitrite to nitric oxide in denitrification, has been extensively studied by synchrotron radiation crystallography (SRX). Although catalytic Cu (Type 2 copper (T2Cu)) of CuNiR had been suspected to tolerate X-ray photoreduction, we here showed that T2Cu in the form free of nitrite is reduced and changes its coordination structure in SRX. Moreover, we determined the completely oxidized CuNiR structure at 1.43 Å resolution with SFX. Comparison between the high-resolution SFX and SRX data revealed the subtle structural change of a catalytic His residue by X-ray photoreduction. This finding, which SRX has failed to uncover, provides new insight into the reaction mechanism of CuNiR.

Keywords: copper/electron transfer/enzyme/serial femtosecond crystallography/X-ray free-electron laser.

Abbreviations: CuNiR, copper nitrite reductase; ET, electron transfer; *Gt*NiR, *Geobacillus thermodenitrificans* copper nitrite reductase; PCET, proton-coupled electron transfer; RT, room temperature; SFX, serial femtosecond crystallography; SRX, synchrotron radiation crystallography; T1Cu, Type 1 copper; T2Cu, Type 2 copper; XFEL, X-ray free-electron laser.

Since the invention of the Haber–Bosch process, the amount of nitrogen oxides fixed in soils and waters has been increasing and the global nitrogen cycle has gradually changed (*1*, *2*). In the cycle, nitrogen fixed in the form of ammonium salts are converted to nitrogen oxides and then reduced to a dinitrogen gas in a stepwise manner ($NO_3^- \rightarrow NO_2^- \rightarrow NO \rightarrow N_2O \rightarrow N_2$) (*3*). This reduction process, denitrification, is the main path for fixed nitrogen to be removed and hence has major agronomic and environmental impacts. Chemical reactions in denitrification are performed by microorganisms and coupled with their anaerobic respiratory systems in which metalloenzymes are utilized (*3*, *4*). Nitrite reduction to nitric oxide ($NO_2^- + e^- + 2H^+ \rightarrow NO + H_2O$) is an important step in denitrification where the ion is changed to the toxic and highly reactive gas. Two types of dissimilatory nitrite reductase (NiR) have been identified to date (*3*, *4*). One of them is cd_1-type heme nitrite reductase (cd_1NiR), which functions as a homodimer (*5*). The other one is copper nitrite reductase (CuNiR): a homotrimeric copper-containing enzyme. CuNiR can also reduce dioxygen to hydrogen peroxide (*6*, *7*) and catalyse the dismutation of superoxide (*8*). Each monomer of typical CuNiR contains two copper sites: Type 1 Cu (T1Cu) with a Cys–Met–His_2 ligand set and Type 2 Cu (T2Cu) with a His_3 ligand set (*9*–*13*). The T1Cu site accepts an electron from *c*-type cytochromes (*14*, *15*) or blue copper proteins (*6*, *16*, *17*), when CuNiR and the donor protein form a transient electron transfer (ET) complex. The received electrons are

Featured Article

transferred to the T2Cu site, the catalytic centre, through a Cys–His pathway. The Asp–His pair (Asp^{cat} and His^{cat}), which is conserved above the T2Cu site and connected via a water molecule (bridging water), is essential to the enzymatic activity (*18*, *19*), though the exact role has been ambiguous.

In conventional synchrotron radiation crystallography (SRX), strong X-ray beams induce photoreduction of metal centres and destroy their natural structures (*20*–*23*). Spectroscopic analysis revealed that T1Cu in CuNiR is rapidly reduced by synchrotron X-ray (*24*). T2Cu is more resistant, than T1Cu, to X-ray damage in the absence of NO_2^-. When the substrate binds to T2Cu, X-ray photoreduction of T1Cu is followed by ET from T1Cu to T2Cu, which results in reduction of NO_2^- *in crystallo* (*24*). This gated ET is explained by the concept of proton-coupled ET (*25*, *26*), although the detailed mechanism remains to be elucidated. Because the presence of NO_2^- accelerates intramolecular ET also in solution (*25*–*27*), it is obvious that ET from T1Cu to T2Cu is gated to some extent. However, kinetic studies demonstrated the random sequential mechanism of nitrite reduction; *i.e*. intramolecular ET can occur both with and without the binding of the substrate (*28*, *29*). Especially, intramolecular ET before substrate binding is dominant at low pH (<6.5) (*28*). Moreover, we have recently shown that substrate-free T2Cu in a CuNiR crystal crystallized at pH 4.5 may be reduced by synchrotron X-rays and that an unknown chemical reaction occurs on T2Cu during data collection (*30*).

To investigate the nitrite reduction mechanism in CuNiR, detailed structural comparison between its oxidized and reduced state is necessary. Here, we closely examined X-ray-induced structural changes and chemical reactions at the T2Cu site using a helical scan method combined with microfocus X-ray beams (*31*). Furthermore, we determined the first completely oxidized CuNiR structure using serial femtosecond crystallography (SFX) with X-ray free-electron laser (XFEL) (*32*), which has enabled damage-free structural determination of metalloenzymes even at room temperature (RT) (*33*–*37*). Because the Bragg spacings of previously determined SFX structures of metalloenzymes were longer than typical covalent bond lengths found in macromolecules (~1.5 Å), it has been difficult to obtain, at the chemical level, new structural insights into the reaction mechanisms of metalloenzymes. CuNiR crystals used in this study have been known to diffract X-rays well; therefore, we could determine its high-resolution SFX structure. We here would like to report our results in detail.

Materials and Methods

Sample preparation of CuNiR from Geobacillus thermodenitrificans (GtNiR)

Geobacillus thermodenitrificans copper nitrite reductase (*Gt*NiR) was expressed and purified as described previously (*30*). We used chloride-free buffers for all the steps of purification and crystallization. Microcrystals for SFX were obtained by a rotational crystallization technique using nanoseeds of the protein as follows. Macrocrystals were transferred to a 1.5 ml tube (Eppendorf, Hamburg, Germany) containing 1 ml of solution composed of 100 mM sodium acetate buffer (pH 4.5), 5.5% (w/v) polyethylene glycol 4,000 and 75 mM $CuSO_4$. After sonicating the crystals on ice with a UD-211 ultrasonicator (Tomy Seiko Co., Tokyo, Japan), the solution was centrifuged and the supernatant was collected as a nanoseed solution. In a 15 ml centrifuge tube (AS ONE Co., Osaka, Japan), 4 ml of the 20 mg/ml protein solution was mixed with 4 ml of the precipitant solution, which was composed of 100 mM sodium acetate buffer (pH 4.5), 15% (w/v) polyethylene glycol 4,000, 75 mM $CuSO_4$ and then 160 µl of the nanoseed solution was added. The centrifuge tube had been rotated on a RT-50 culture rotator (TITEC, Saitama, Japan) at ~30 rpm for 1 week at RT. The microcrystal solution was filtered through a 30 µm CellTrics filter (Chiyoda Sci. Co., Tokyo, Japan) and adjusted to a number density of $\sim 4.4 \times 10^8$ crystals/ml by adding 4 ml of the precipitant solution.

Synchrotron data collection

Cryogenic SRX datasets were collected using microfocus beamline BL32XU at SPring-8 (*38*). A large single crystal of *Gt*NiR ($915 \times 620 \times 230\ \mu m^3$) was flash-cooled by immersion in liquid nitrogen and mounted on a conventional goniometer with the longest axis roughly directed towards the horizontal rotation axis. Along the longest edge of the crystal, 120 irradiation points were chosen. The regular intervals between the irradiation points were 7.6 µm, which is sufficient to separate the radiation damage at each irradiation point. The beam at a wavelength of 0.7500 Å was focused to 15 µm (height, H) × 1.0 µm (width, W) with a photon flux of 8×10^{11} photons/s. Using the helical scan method, a total of seven datasets (SR1–SR7) were repeatedly collected in order from the same points of the same crystal except for absorbed X-ray dose per frame. The exposure time for each image was 1 s. For datasets SR1, SR3, SR5 and SR7, each image was collected with an absorbed dose of 0.064 MGy/frame with a 92.3% attenuated beam, while for datasets SR2, SR4 and SR6, the dose corresponded to 8.252 MGy/frame without attenuation. The X-ray doses were calculated with RADDOSE (*39*). The parameters and statistics are summarized in Table I.

RT data collection was performed at BL38B1 of SPring-8 (*40*), as described previously (*41*). The dataset was collected from one position of a single crystal using an ADSC Quantum 315 charge-coupled device (CCD) detector (Area Detector Systems Co., CA, USA). The beam size was 50 µm (H) × 88 µm (W). The oscillation angle and exposure time per image were set to 1° and 1.5 s, respectively. A total of 120 diffraction images were collected from the single crystal. The parameters and statistics are summarized in Table II.

Structure determination of the SRX structures

All of the datasets were indexed and integrated using HKL2000 (*42*). The phases were determined by the molecular replacement method using MOLREP (*43*) with a *Gt*NiR monomer (Protein Data Bank (PDB) code 4ZK8) as a search model. Manual model building was performed using WinCoot 0.7 (*44*). The program REFMAC5 (*45*) from the CCP4 suite (ver. 6.5.0) (*46*) was used for structural refinement. Anisotropic displacement parameters were introduced after water molecules were built in the models. The final models were checked for stereochemical quality using MolProbity (*47*).

Single-shot XFEL data collection

The experiment was performed at BL3 of SPring-8 Angstrom Compact Free-Electron Laser (SACLA) in Hyogo, Japan (*48*). Using 2–10 fs XFEL pulses, we collected diffraction patterns from greenish-blue (aerobically oxidized) *Gt*NiR microcrystals (Supplementary Fig. S1a). The pulse duration shorter than 10 fs is quite important to obtain intact metalloprotein structures, because ultrabright XFEL beams damage electronic structures of heavy atoms in a few tens of femtoseconds (*49*) and can destroy the natural structures of metal centres (*50*). A liquid injector (nozzle aperture diameter: 200 µm) with a sample circulation system was used (*51*). Microcrystal sample (5.5 ml) was placed in a reservoir. The flow rate was set to 5.3 ml/min (70 cm/s). The injector was installed in a helium ambiance, diffraction chamber enclosure: Diverse Application Platform for Hard X-ray Diffraction in SACLA (DAPHNIS) (*52*). The liquid–stream width was nearly the same as the aperture size. The sample chamber was maintained at a temperature of 300 K with a humidity of 85–99%. The diffraction patterns were collected using a short-working-distance octal multiport CCD detector (*53*) with

Table I. Data collection and refinement statistics for the cryogenic SRX structures

Name/PDB ID	SR1/4YSO	SR2/4YSP	SR3/4YSQ	SR4/4YSR	SR5/4YSS	SR6/4YST	SR7/4YSU
Data collection at BL32XU of SPring-8 (Wavelength 0.7500 Å)							
X-ray dose (MGy)	0.064	8.316	8.380	16.632	16.696	24.948	25.012
Space group	*R*3	*R*3	*R*3	*R*3	*R*3	*R*3	*R*3
Unit cell $a = b$, c (Å)	114.8, 84.10	114.9, 84.23	115.0, 84.23	115.0, 84.34	115.1, 84.31	115.2, 84.38	115.2, 84.39
Resolution (Å)	50.0–1.50 (1.55–1.50)	50.0–1.34 (1.39–1.34)	50.0–1.50 (1.55–1.50)	50.0–1.34 (1.39–1.34)	50.0–1.50 (1.55–1.50)	50.0–1.34 (1.39–1.34)	50.0–1.50 (1.55–1.50)
R_{sym} (%)	10.9 (53.3)	9.8 (31.2)	10.7 (55.0)	10.1 (30.5)	11.7 (64.4)	12.2 (36.9)	13.9 (78.7)
R_{pim} (%)	7.4 (35.1)	6.7 (17.5)	7.4 (36.7)	7.1 (21.0)	8.0 (43.4)	8.3 (25.4)	9.5 (55.0)
$CC_{1/2}$	(0.530)	(0.895)	(0.576)	(0.871)	(0.465)	(0.810)	(0.277)
Completeness (%)	96.9 (98.5)	93.6 (98.2)	96.6 (98.6)	92.8 (98.0)	96.4 (98.6)	93.1 (98.1)	96.1 (97.4)
Unique reflections	63,495 (6,470)	87,908 (9,204)	64,868 (6,624)	87,653 (9,255)	64,668 (6,623)	88,348 (9,311)	64,638 (6,537)
$\langle I/\sigma\,(I)\rangle$	12.2 (2.77)	11.8 (6.03)	11.2 (2.01)	11.3 (4.66)	10.0 (1.60)	8.77 (3.53)	8.05 (1.34)
Redundancy	3.0 (3.0)	3.1 (3.0)	2.9 (3.0)	3.0 (3.0)	2.9 (3.0)	3.0 (2.9)	2.8 (2.8)
Refinement							
Resolution (Å)	38.73–1.50 (1.54–1.50)	20.08–1.34 (1.37–1.34)	34.35–1.50 (1.53–1.50)	50.00–1.34 (1.37–1.34)	33.23–1.50 (1.54–1.50)	20.12–1.34 (1.37–1.34)	42.94–1.50 (1.54–1.50)
R_{work}/R_{free} (%)	12.9/17.7	12.6/15.0	14.0/18.7	14.3/17.4	14.8/19.1	15.5/18.5	16.3/20.8
No. of							
protein atoms	2,375	2,383	2,344	2,352	2,377	2,355	2,359
ligand/ions	20	20	28	20	28	19	18
water	371	294	331	302	311	294	273
Average B (Å^2)							
All	13.9	13.8	19.0	14.7	16.3	17.1	16.2
Protein atoms	11.7	12.3	17.1	12.8	14.7	15.5	14.7
Water atoms	26.8	24.5	31.5	28.2	27.5	29.2	26.1
T1Cu, T2Cu	8.6, 8.7	9.6, 8.7	14.0, 13.3	9.83, 9.13	11.4, 10.7	12.2, 11.7	10.8, 10.6
Other atoms	29.6	31.2	32.8	32.6	33.5	35.9	38.6
Ramachandran							
Favoured (%)	98.0	97.7	98.3	98.0	98.0	97.3	97.3
Allowed (%)	2.0	2.3	1.7	2.0	2.0	2.7	2.7
Outliers (%)	0	0	0	0	0	0	0

Table II. Data collection and refinement statistics for the RT SRX structure

Data collection at BL38B1 of SPring-8 (Wavelength 0.9000 Å)	
Space group	*R*3
Unit cell $a = b$, c (Å)	116.2, 85.55
Resolution range (Å)	50.0–1.35 (1.55–1.35)
R_{sym} (%)	9.6 (36.2)
Completeness (%)	99.8 (100)
Unique reflections	94,321 (4,709)
$\langle I/\sigma\,(I)\rangle$	24.4 (2.4)
Redundancy	4.2 (3.6)
Refinement	
Resolution (Å)	26.5–1.35 (1.39–1.35)
R_{work} (%)/R_{free} (%)	9.7/12.0
No. of protein atoms	2,574
No. of ligand atoms and ions	17
No. of water molecules	219
Average B (Å^2)	
All	18.9
Protein atoms	17.6
Water	34.1
T1Cu atom	11.6
T2Cu atom	10.5
Other atoms	26.8
Ramachandran plot (%)	
Favoured	97.3
Allowed	2.7
Outliers	0
Coordinate error (Å)	0.020
PDB code	4YSD

XFEL radiation. The microcrystals were exposed to single X-ray pulses at a photon energy of 11.0 keV. The pulses consisted of 5×10^{10} photons/pulse were focused to 2.5 μm (H) × 2.0 μm (W) at the interaction point using Kirkpatrick–Baez mirrors (*54*). The repetition rate was 30 Hz, and the typical pulse energy at the sample was 90 μJ/pulse. The parameters and statistics are summarized in Table III.

Structural determination of the SFX structure

A total of 180,942 images were collected, of which 139,391 diffraction images were identified and 37,186 images were indexed and merged using CrystFEL (*55*). The data was indexed as space group *R*3 and processed as space group *H*3. Indexing ambiguity in SFX was solved by an algorithm that clusters snapshots (*56*). The phase was determined by molecular replacement using MOLREP with the *Gt*NiR monomeric unit (PDB code 4ZK8) as a search model. Manual model building was performed using WinCoot 0.7. The program REFMAC5 from the CCP4 suite (ver. 6.5.0) was used for structure refinement. The microcrystals diffracted X-rays beyond 1.4 Å resolution (Supplementary Fig. S1b) but the statistics of high-resolution shells, such as $CC_{1/2}$ and R_{split}, were poor (Supplementary Fig. S2). We therefore performed paired refinement to determine the 'nominal resolution', based on the idea that proper use of weaker and noisier but higher-resolution data can provide better models (*57*, *58*). Actually, inclusion of noisy high-resolution data enables the better analysis of SFX data (*59*). The result of paired refinement showed that including higher-resolution data provided a better model than rejecting it (Supplementary Fig. S3a). The student's *t*-test *P* value calculated from $CC_{1/2}$ in the highest resolution shell cut at 1.43 Å resolution (0.0417, $n = 7{,}859$) was 0.000214, which is less than the significance level $\alpha = 0.001$ (Supplementary Fig. S3b). Conversely, the *P* value calculated from $CC_{1/2}$ in the highest resolution shell cut at 1.42 Å resolution (0.0246, $n = 8{,}164$) was 0.0261, which is greater than α (Supplementary Fig. S3b). Based on these things, we chose to use data up to 1.43 Å resolution, and performed further refinement. The final model was checked for stereochemical quality using MolProbity.

Results

Radiation damages to GtNiR in SRX

The structures for SR1, SR3, SR5 and SR7 data were refined against data to 1.50 Å resolution, whereas those for SR2, SR4 and SR6 data were refined to 1.34 Å resolution (Table I). Root-mean-square deviations (RMSDs) for C^{α} atoms between seven structures were at most 0.1 Å.

Table III. Data collection and refinement statistics for the SFX structure

Data collection	
Beamline	SACLA BL3
Wavelength (Å)	1.129
Space group	*R*3
Unit cell $a = b$, c (Å)	116.2, 85.55
Resolution range (Å)	34.8–1.43 (1.47–1.43)
R_{split} (%)	17.70 (113.8)
Completeness (%)	100 (99.97)
Unique reflections	79,590 (7,859)
$CC_{1/2}$	0.970 (0.0417)
$<I/\sigma\ (I)>$	3.38 (0.99)
Redundancy	245.3 (207.0)
Refinement	
Resolution range (Å)	34.80–1.43 (1.47–1.43)
R_{work} (%)/R_{free} (%)	13.7/14.9
No. of protein atoms	2,414
No. of heterogen atoms	9
No. of water molecules	134
Average B (Å^2)	
All	24.0
Protein atoms	23.3
Water	36.6
T1Cu	20.4
T2Cu	17.9
Other atoms	31.7
Ramachandran plot (%)	
Favoured	96.4
Allowed	3.6
Outliers	0
PDB code	4YSA

Changes in ligand–T1Cu distance fell within the range of coordinate errors (Table IV), indicating that the T1Cu site did not show significant structural changes that can be detected at resolutions of our present structures. Conversely, the T2Cu site showed obvious structural changes induced by X-ray irradiation: two water ligands (WatC and WatD) were present on T2Cu in the SR1 structure, while the electron density of WatD was not observed in other SR data (Fig. 1a). Furthermore, with increasing X-ray dose, the T2Cu atom gradually sank towards a 'ligand plane' composed of three $N^{\varepsilon 2}$ atoms of His ligands (Fig. 1b and c).

Completely oxidized GtNiR structure determined by SFX

The SFX structure was refined to 1.43 Å resolution (Table III, see Materials and Methods). The final R_{work} and R_{free} values were 13.7 and 14.9%, respectively, showing that the model has a good agreement with the experimental data. RMSDs of C^{α} atoms between the SFX structure and cryogenic SRX structures were <0.2 Å. Anomalous peaks of T1Cu and T2Cu were clearly observed (Fig. 2a). The ligand–T1Cu distances in the SFX structure were the same as those in the SRX structures within the range of coordinate errors (Table IV). T2Cu in the SFX structure was coordinated by three histidine residues, WatC and WatD (Fig. 2b). The distance from T2Cu to the ligand plane was longer than those of the SRX structures (Fig. 1c), although it is almost the same as that in the SR1 structure within the range of coordinate errors.

An unidentified electron density was observed in the vicinity of T2Cu–ligand water molecules in the SFX data (Fig. 2b). We tentatively assigned this to a 40% occupancy sodium ion (Na^+) from the crystallization buffer for the following reasons. The peak assigned to Na^+ was close to WatB, WatC, WatD and Asp98 (Asp^{cat}) as shown in Fig. 2c. The distances from the assigned Na^+ to water molecules or Asp98 were shorter than typical hydrogen bonds but longer than typical covalent bonds in protein crystal structures. We could rule out a disordered water model because all water molecules in Fig. 2c showed full occupancy. It is, therefore, reasonable to speculate that the atom at the peak is a metal ion and forms coordination bonds with water and Asp^{cat}. The peak did not show an anomalous peak, meaning that it is not Cu. Na^+ was the only metal ion, other than Cu, in the crystallization solution. Furthermore, Asp^{cat} can easily form a coordination bond with a cation because it is deprotonated in the resting state (*60*).

Presumably because of the high concentration of $CuSO_4$ in the crystallization buffer, there existed an anomalous peak of 20% occupancy Cu bound to His244 (His^{cat}) in the SFX data (Fig. 2a, Supplementary Fig. S5). Because the Cu atom was very close to bridging water (1.44 Å, Supplementary Fig. S5), we regarded the Cu atom and bridging water were alternative structures. The occupancy of bridging water was 80%. This anomalous peak of Cu was also observed in a previously determined cryogenic SRX structure (PDB code 3X1E, Supplementary Fig. S6). CuNiR has evolutionary and structural relationship with some multicopper oxidases (MCOs) (*61–64*), and His^{cat} in CuNiR is superimposed to one of the His ligands to a trinuclear copper centre in the MCOs (*63*, *64*). Therefore, the binding of extra Cu to His^{cat} is not a surprising phenomenon.

RT SRX structure of GtNiR

Cryo-manipulations of protein crystals in SRX can change the population of amino acid side chains (*65*, *66*). Due to its thermostability, *Gt*NiR macrocrystals can be used in SRX without cryo-cooling (*41*); therefore, we determined an RT SRX structure of *Gt*NiR to judge whether the observed structural differences between cryogenic SRX and SFX structures were derived from X-ray photoreduction and not from the difference of measurement temperatures. The RT SRX structure was refined to 1.35 Å resolution (Table II). The final R_{work} and R_{free} values were 9.7 and 12.0%, respectively. RMSDs of C^{α} atoms between the RT SRX and cryogenic SRX structures were <0.2 Å. The RMSD of C^{α} atoms between the RT SRX and SFX structure was 0.08 Å.

The T2Cu in the RT SRX structure was coordinated by three His ligands and two water molecules (Supplementary Fig. S7). The distance from T2Cu to the ligand plane was shorter than that of the SR1 structure and longer than those of other SRX structures (Fig. 1c), albeit within the range of errors. However, it is obvious that the distance was shorter

Table IV. Coordination geometries of the copper sites

	SFX	SR1	SR2	SR3	SR4	SR5	SR6	SR7
Coordinate error (Å)	0.012	0.042	0.021	0.048	0.025	0.052	0.029	0.062
I. T1Cu–Ligand Distances (Å)								
Cu-H95N$^{\delta1}$	2.03	2.02	2.04	2.01	2.03	2.03	2.06	2.05
Cu-C135S$^{\gamma}$	2.27	2.21	2.23	2.25	2.25	2.25	2.22	2.22
Cu-H143N$^{\delta1}$	1.91	1.97	2.05	2.02	2.02	2.04	2.03	2.03
Cu-M148S$^{\delta}$	2.66	2.70	2.64	2.67	2.64	2.67	2.61	2.67
II. T1Cu–Ligand Angles (°)								
H95-Cu-C135	135.3	136.6	134.3	133.4	133.1	132.9	133.2	134.2
H95-Cu-H143	104.5	102.6	104.2	106.0	105.2	105.1	105.4	104.0
His95-Cu-M148	81.1	82.1	81.5	82.1	82.1	84.1	80.8	82.1
C135-Cu-H143	105.8	105.1	106.8	106.9	106.7	105.7	105.5	106.1
C135-Cu-M148	110.2	109.8	112.1	111.8	111.6	112.0	112.9	113.6
H143-Cu-M148	120.2	121.8	116.9	115.2	117.3	116.4	118.7	115.9
III. T2Cu–Ligand Distances (Å)								
Cu-H100N$^{\varepsilon2}$	2.07	2.07	2.04	2.09	2.07	2.02	2.04	2.03
Cu-H134N$^{\varepsilon2}$	2.12	1.99	2.01	2.03	1.98	2.01	1.97	2.01
Cu-H294N$^{\varepsilon2}$	2.02	2.06	1.99	2.01	1.99	2.04	2.01	2.01
IV. T2Cu–Ligand Angles (°)								
H100-Cu-H134	106.0	106.0	113.6	115.2	116.1	116.1	115.3	114.2
H100-Cu-H294	97.24	97.72	99.9	102.7	100.7	102.6	101.3	104.3
H134-Cu-H294	106.3	108.2	111.0	110.5	112.4	111.7	111.9	111.9
V. Distances from T2Cu to the ligand planes (Å)								
	0.881	0.845	0.703	0.678	0.657	0.648	0.663	0.642

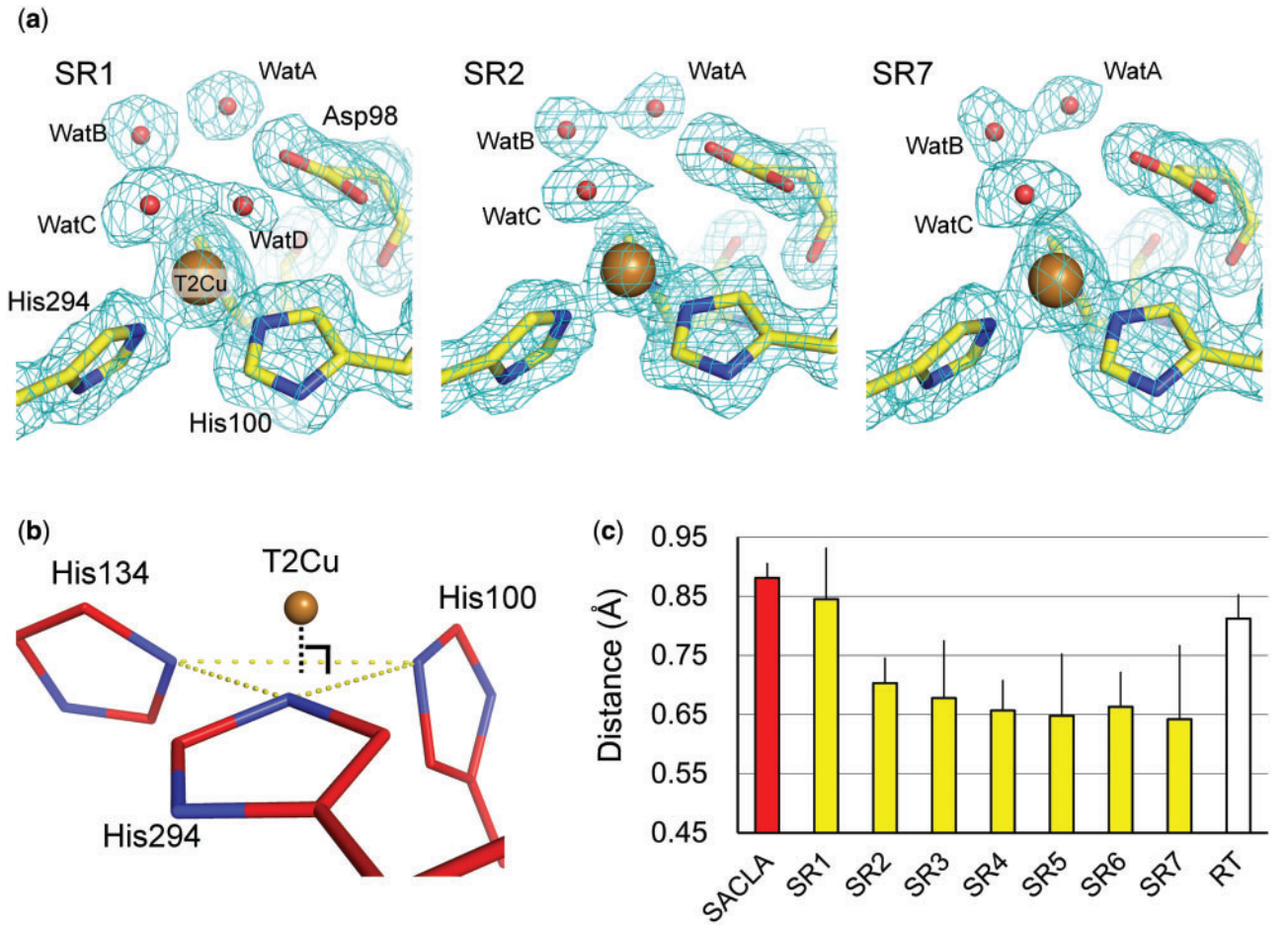

Fig. 1 Structural changes in SRX. (**a**) Changes in the hydration structures at the T2Cu site. The $2F_o$–F_c maps contoured at 1.0 σ are shown as cyan meshes. Carbon, oxygen, nitrogen and copper atoms are yellow, red, blue and brown, respectively. (**b**) The ligand plane composed of three N$^{\varepsilon2}$ atoms of His residues at the T2Cu site (yellow-dashed lines). Carbon, nitrogen and copper atoms are coloured in bright red, blue and brown, respectively. (**c**) Distances from T2Cu to the ligand plane. The error bars represent twice the values of the coordinate errors estimated by the maximum likelihood method. (A colour version of this figure is available online at: http://jb.oxfordjournals.org)

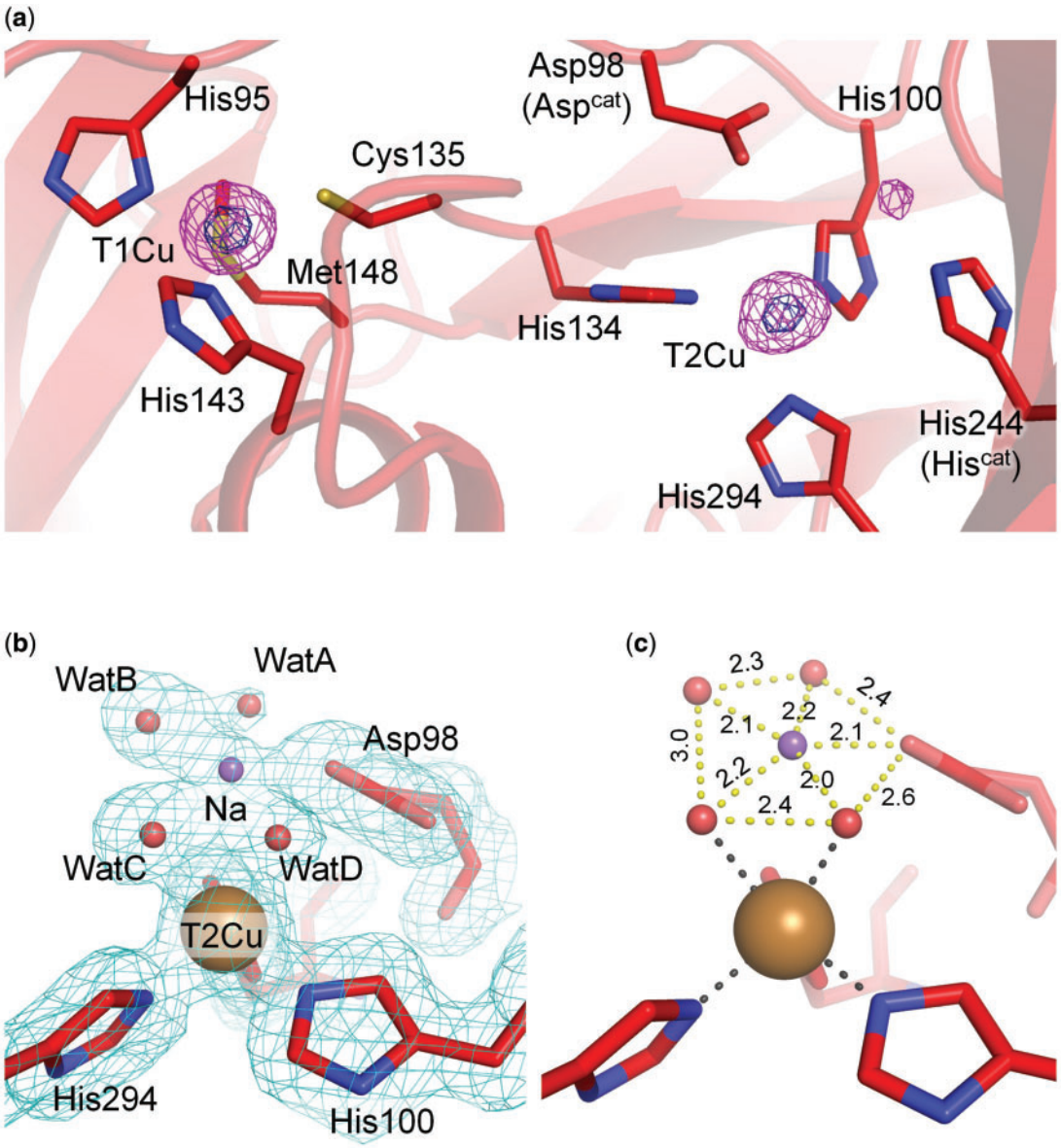

Fig. 2 SFX structure of *Gt*NiR. Carbon, oxygen, nitrogen, sulfur and copper atoms are bright red, red, blue, yellow and brown, respectively. (**a**) Copper binding sites in the SFX structure. The anomalous Fourier maps are contoured at 4.0 (magenta) and 12 σ (dark blue). (**b**) Hydration structure of the T2Cu site in the SFX structure. The $2F_o$–F_c maps contoured at 1.0 σ are shown as cyan meshes. Na^+ and water molecules are shown as a purple sphere. (**c**) Penta-coordinated Na^+ above the T2Cu site. Distances are shown in Å. (A colour version of this figure is available online at: http://jb.oxfordjournals.org)

than that in the SFX structure. The electron density map of the RT SRX data has a strong positive peak around WatC with full occupancy (Supplementary Fig. S4c). We also observed an unidentified positive electron density peak (Supplementary Fig. S4c) at the corresponding position of the putative Na^+ site in the SFX structure (Supplementary Fig. S4b), though the signal was too weak to place any atomic model there. The observation that both RT SRX and SFX data show this electron density means, at least, that it is not the result of photoreduction.

The electron density map of the RT SRX data showed a strong electron density peak near His^{cat}. When water is assigned there, the modelled molecule was too close to His^{cat} (<2.0 Å). Therefore, it was likely to be a Cu ion coordinated by His^{cat} (Supplementary Fig. S7) as was observed in the SFX structure and the 3X1E structure.

Redox-coupled conformational change in His^{cat}

Compared with the SFX structure, cryogenic and RT SRX structures revealed that the imidazole ring and the C^{β} atom of His^{cat} rotated ~10° and moved 0.3 Å, respectively (Fig. 3a and b, Supplementary Fig. S8). To confirm that it is not the result of cutting the SFX data at 1.43 Å resolution, we refined the SFX structure against the data to 1.65 Å resolution, where $CC_{1/2} \sim 0.5$ and $R_{split} < 100$ (Supplementary Fig. S2), and the conformation of His^{cat} did not change (Supplementary Fig. S9). The $N^{\delta 1}$ atom of His^{cat} forms a bifurcated

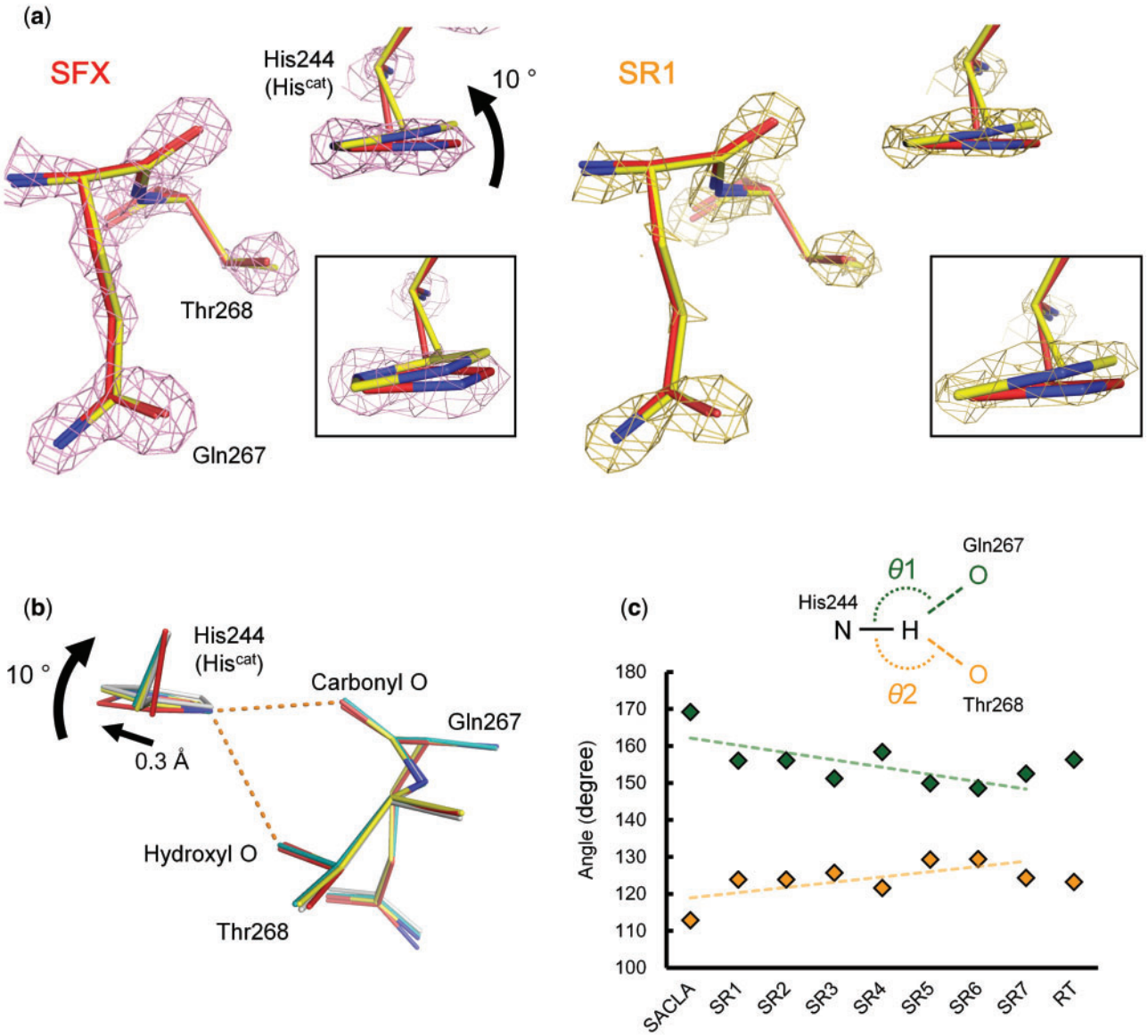

Fig. 3 Redox-coupled rotation of His^{cat}. (**a**) Electron density maps (contoured at 4.0 σ) around His^{cat} in the SFX (red) and SR1 (yellow) structures. (**b**) Comparison of His^{cat} of the SFX (red), SR1 (yellow), SR7 (teal blue) and RT SRX (white) structures. (**c**) Changes in the angle of the bifurcated hydrogen bond. The upper and lower series show θ1 and θ2, respectively. Trends are shown by dashed lines. (A colour version of this figure is available online at: http://jb.oxfordjournals.org)

hydrogen bond with the hydroxyl oxygen atom of Thr268 and the backbone carbonyl oxygen atom of Gln267 (Fig. 3b). The His^{cat} rotation changes the states of the bifurcated hydrogen bond. To qualitatively evaluate this subtle change, we modelled hydrogen atoms of His^{cat} at the ideal positions without refinement. Figure 3c shows that with increasing of X-ray dose, the θ1 ($N^{\delta1}$–H–O_{Gln}) angle and the θ2 ($N^{\delta1}$–H–O_{Thr}) angle decreased and increased, respectively.

Discussion

Geometrical changes at Cu sites

We recently demonstrated that T1Cu in a *Gt*NiR crystal is reduced by at least an X-ray dose of 0.041 Mgy (*30*). Because even the X-ray dose for SR1 was higher than this value (Table I), T1Cu in the present SRX structures must be, more or less, reduced. However, the geometries around T1Cu did not show significant differences between the SRX structures and the completely oxidized SFX structure (Table IV). It is not surprising because spectroscopic studies have revealed that the typical changes in ligand–T1Cu distance in reduction are <0.1 Å so as to minimize the reorganization energy in ET (*67*).

We revealed that X-ray irradiation made the T2Cu atom gradually move towards to the ligand plane (Fig. 1c). Sunken T2Cu atoms have been observed in the reduced forms of other CuNiRs (*68–70*). Therefore, contrary to the previous report (*24*), our result indicates that T2Cu free of NO_2^- can be reduced in SRX. This conclusion is reasonable because our crystal was crystallized at a pH low enough (pH 4.5) for intramolecular ET without NO_2^- binding to occur dominantly (*28*). Although the T2Cu sites in CuNiR

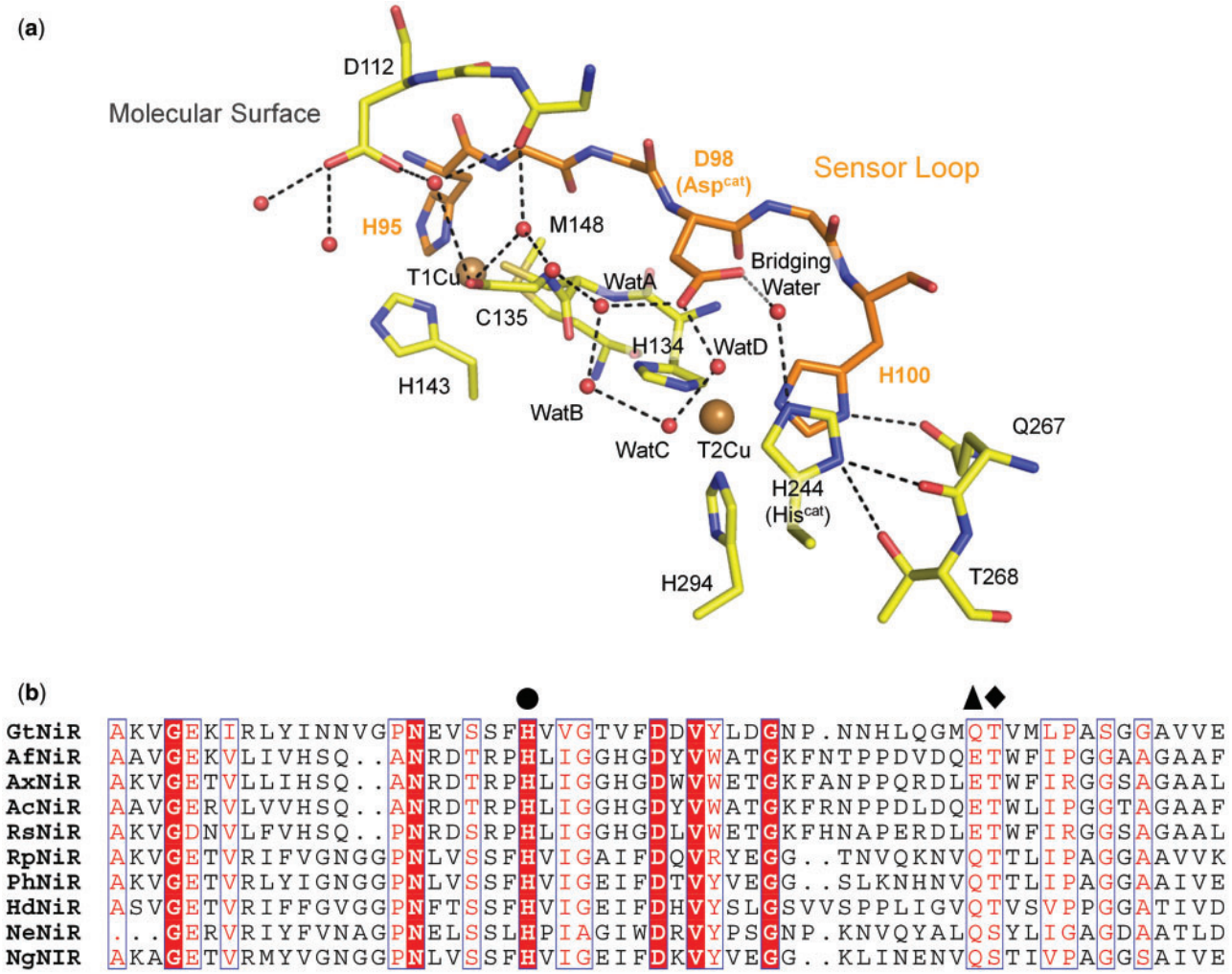

Fig. 4 Conserved hydrogen bond network. (**a**) Redox sensor loop in *Gt*NiR. The hydrogen bond network is shown by dotted lines. (**b**) Amino acid sequences of CuNiRs. His^{cat}, Gln/Glu and Thr/Ser are indicated by filled circle, triangle and diamond, respectively. Ax, Ac, Rs, Rp, Ph and Hd means *Achromobacter xylosoxidans*, *Achromobacter cycloclastes*, *Rhodobacter sphaeroides*, *Ralstonia pickettii*, *Pseudoalteromonas haloplanktis* and *Hyphomicrobium denitrificans*, respectively. (A colour version of this figure is available online at: http://jb.oxfordjournals.org)

crystals lose ligand water when it is harshly reduced by artificial reductants (*68*–*70*), it is just one of the reduced states of T2Cu, called inactive reduced state, and a normal reduced state retains water ligand (*29*) as was observed in our structures (Fig. 1a).

Conformational change of His^{cat}

The structural change of His^{cat} cannot be caused by coordination of Cu or the presence of Na^+ above the T2Cu site, because the former was found also in the cryogenic and RT SR structures (Supplementary Fig. S6 and S7) and the latter was found also in the RT SR structure (Supplementary Fig. S4c). The difference of measurement temperature is not a major cause of the structural change (Fig. 3b). Thus, the conformational difference in His^{cat} between the SFX and SRX structures is most likely to result from photoreduction of the Cu sites. Indeed, the observed conformational change was small and is probably due to the rigid catalytic site of thermostable *Gt*NiR (*71*).

Interestingly, there is a hydrogen bond between T2Cu ligand His100 and the side chain of Gln267, and His100 is located at the end of a sensor loop (Fig. 4a), which is thought to transmit information about T1Cu's redox state to T2Cu (*8*, *72*). Although the Thr–Gln pair (or Thr–Glu in some CuNiRs) composing the bifurcated hydrogen bond has been ignored for long, they are conserved in CuNiRs except for a few CuNiRs, which have Ser at the position of Thr (Fig. 4b). The nitrite reduction activity of Ser-containing CuNiR is lower than the activity of Thr-containing CuNiR (*70*, *73*). The crystal structures of Ser-containing CuNiRs show that the Ser residue does not always form a hydrogen bond with His^{cat} (*70*, *73*). These facts imply the enzymatic importance of the hydrogen bond between His^{cat} and Thr.

The rotation of the imidazole ring changes the θ angles of the bifurcated hydrogen bond (Fig. 3c). Generally, the θ angle is used as an indicator of hydrogen bond strength. Strong, moderate and weak hydrogen bonds tend to show 170–180°, 150–180°, 90–150° θ angles, respectively (*74*). Therefore, the His^{cat} rotation strengthens the hydrogen bond between His^{cat} and Thr and weakens the hydrogen bond between His^{cat}

and Gln/Glu. Because the hydroxyl oxygen atom is less negatively polarized than the carbonyl oxygen atom, this structural change may destabilize the positive charge on His^{cat}, which may facilitate transfer of a proton to the bridging water between Asp^{cat} and His^{cat} (Fig. 4a). His^{cat} has been suggested to directly provide a proton to NO_2^- (*19*, *75*); however, our results indicate another possibility. His^{cat} may function as a switch for proton relay.

Supplementary Data

Supplementary Data are available at *JB* Online.

Acknowledgements

The SFX experiment was carried out at BL3 of the SPring-8 Angstrom Compact Free-Electron Laser (SACLA) with the approval of the Japan Synchrotron Radiation Research Institute (JASRI) (proposal no. 2013B8045). We are grateful for support from the SACLA High Performance Computing (HPC) system and the Mini-K super computer system. The microfocus SRX experiment at BL32XU of SPring-8 was supported by the Platform for Drug Discovery, Informatics and Structural Life Science. The authors thank M.E.P. Murphy for discussion; K. Baba and N. Mizuno for their help in the experiment at BL38B1 (proposal no. 2013A1592); E. Yamashita and A. Higashiura for their support at BL44XU of the SPring-8 and all staff at the SACLA for technical assistance.

Funding

This work was supported by the X-ray Free-Electron Laser Priority Strategy Program of the Ministry of Education, Culture, Sports, Science and Technology in Japan (MEXT), the Grant-in-Aid for Scientific Research on Innovative Areas from MEXT, the Grant-in-Aid for Japan Society for the Promotion of Science (JSPS) Research Fellows (Grant no. 254626), and the JSPS KAKENHI (Grant no. 15K18487).

Conflict of Interest

None declared.

References

1. Gruber, N. and Galloway, J.N. (2008) An Earth-system perspective of the global nitrogen cycle. *Nature* **451**, 293–296
2. Galloway, J.N., Townsend, A.R., Erisman, J.W., Bekunda, M., Cai, Z., Freney, J.R., Martinelli, L.A., Seitzinger, S.P., and Sutton, M.A. (2008) Transformation of the nitrogen cycle: recent trends, questions, and potential solutions. *Science* **320**, 889–892
3. Zumft, W.G. (1997) Cell biology and molecular basis of denitrification. *Microbiol. Mol. Biol. Rev.* **61**, 533–616
4. Tavares, P., Pereira, A.S., Moura, J.J., and Moura, I. (2006) Metalloenzymes of the denitrification pathway. *J. Inorg. Biochem.* **100**, 2087–2100
5. Fülöp, V., Moir, J.W.B., Ferguson, S.J., and Hajdu, J. (1995) The anatomy of a bifunctional enzyme: structural basis for reduction of oxygen to water and synthesis of nitric oxide by cytochrome cd_1. *Cell* **81**, 369–377
6. Kakutani, T., Watanabe, H., Arima, K., and Beppu, T. (1981) A blue protein as inactivating factor for nitrite reductase from *Alcaligenes faecalis* Strain S-6. *J. Biochem.* **89**, 463–472
7. MacPherson, I.S., Rosell, F.I., Scofield, M., Mauk, A.G., and Murphy, M.E. (2010) Directed evolution of copper nitrite reductase to a chromogenic reductant. *Protein Eng. Des. Sel.* **23**, 137–145
8. Strange, R.W., Murphy, L.M., Dodd, F.E., Abraham, Z.H.L., Eady, R.R., Smith, B.E., and Hasnain, S.S. (1999) Structural and kinetic evidence for an ordered mechanism of copper nitrite reductase. *J. Mol. Biol.* **287**, 1001–1009
9. Godden, J., Turley, S., Teller, D., Adman, E., Liu, M., Payne, W., and LeGall, J. (1991) The 2.3 angstrom X-ray structure of nitrite reductase from *Achromobacter cycloclastes*. *Science* **253**, 438–442
10. Kukimoto, M., Nishiyama, M., Murphy, M.E.P., Turley, S., Adman, E.T., Horinouchi, S., and Beppu, T. (1994) X-ray structure and site-directed mutagenesis of a nitrite reductase from *Alcaligenes Faecalis* S-6: roles of two copper atoms in nitrite reduction. *Biochemistry* **33**, 5246–5252
11. Dodd, F.E., Beeumen, J.V., Eady, R.R., and Hasnain, S.S. (1998) X-ray structure of a blue-copper nitrite reductase in two crystal forms. The nature of the copper sites, mode of substrate binding and recognition by redox partner. *J. Mol. Biol.* **282,** 369–382
12. Inoue, T., Gotowda, M., Deligeer, Kataoka, K., Yamaguchi, K., Suzuki, S., Watanabe, H., Gohow, M., and Kai, Y. (1998) Type 1 Cu structure of blue nitrite reductase from *Alcaligenes xylosoxidans* GIFU 1051 at 2.05 Å resolution: comparison of blue and green nitrite reductases. *J. Biochem.* **124**, 876–879
13. Merkle, A.C., and Lehnert, N. (2012) Binding and activation of nitrite and nitric oxide by copper nitrite reductase and corresponding model complexes. *Dalton Trans.* **41**, 3355–3368
14. Koteishi, H., Nojiri, M., Nakagami, T., Yamaguchi, K., and Suzuki, S. (2009) Cytochrome c_{551} is a mediator of electron transfer between copper-containing nitrite reductase and azurin in a denitrifying bacterium, *Achromobacter xylosoxidans*. *Bull. Chem. Soc. Jpn.* **82**, 1003–1005
15. Nojiri, M., Koteishi, H., Nakagami, T., Kobayashi, K., Inoue, T., Yamaguchi, K., and Suzuki, S. (2009) Structural basis of inter-protein electron transfer for nitrite reduction in denitrification. *Nature* **462**, 117–120
16. Vlasie, M.D., Fernandez-Busnadiego, R., Prudencio, M., and Ubbink, M. (2008) Conformation of pseudoazurin in the 152 kDa electron transfer complex with nitrite reductase determined by paramagnetic NMR. *J. Mol. Biol.* **375**, 1405–1415
17. Impagliazzo, A., Blok, A.J., Cliff, M.J., Ladbury, J.E., and Ubbink, M. (2007) Redox-state-dependent complex formation between pseudoazurin and nitrite reductase. *J. Am. Chem. Soc.* **129**, 226–233
18. Boulanger, M.J., Kukimoto, M., Nishiyama, M., Horinouchi, S., and Murphy, M.E. (2000) Catalytic roles for two water bridged residues (Asp-98 and His-255) in the active site of copper-containing nitrite reductase. *J. Biol. Chem.* **275**, 23957–23964
19. Kataoka, K., Furusawa, H., Takagi, K., Yamaguchi, K., and Suzuki, S. (2000) Functional analysis of conserved aspartate and histidine residues located around the type 2 copper site of copper-containing nitrite reductase. *J. Biochem.* **127**, 345–350
20. Yano, J., Kern, J., Irrgang, K.D., Latimer, M.J., Bergmann, U., Glatzel, P., Pushkar, Y., Biesiadka, J., Loll, B., Sauer, K., Messinger, J., Zouni, A., and Yachandra, V.K. (2005) X-ray damage to the Mn_4Ca complex in single crystals of photosystem II: a case

study for metalloprotein crystallography. *Proc. Natl. Acad. Sci. USA* **102**, 12047–12052

21. Schlichting, I., Berendzen, J., Chu, K., Stock, A.M., Maves, S.A., Benson, D.E., Sweet, R.M., Ringe, D., Petsko, G.A., and Sligar, S.G. (2000) The catalytic pathway of cytochrome P450cam at atomic resolution. *Science* **287**, 1615–1622
22. Berglund, G.I., Carlsson, G.H., Smith, A.T., Szöke, H., Henriksen, A., and Hajdu, J. (2002) The catalytic pathway of horseradish peroxidase at high resolution. *Nature* **417**, 463–468
23. Beitlich, T., Kuhnel, K., Schulze-Briese, C., Shoeman, R.L., and Schlichting, I. (2007) Cryoradiolytic reduction of crystalline heme proteins: analysis by UV-Vis spectroscopy and X-ray crystallography. *J. Synch. Rad.* **14**, 11–23
24. Hough, M.A., Antonyuk, S.V., Strange, R.W., Eady, R.R., and Hasnain, S.S. (2008) Crystallography with online optical and X-ray absorption spectroscopies demonstrates an ordered mechanism in copper nitrite reductase. *J. Mol. Biol.* **378**, 353–361
25. Brenner, S., Heyes, D.J., Hay, S., Hough, M.A., Eady, R.R., Hasnain, S.S., and Scrutton, N.S. (2009) Demonstration of proton-coupled electron transfer in the copper-containing nitrite reductases. *J. Biol. Chem.* **284**, 25973–25983
26. Leferink, N.G., Han, C., Antonyuk, S.V., Heyes, D.J., Rigby, S.E., Hough, M.A., Eady, R.R., Scrutton, N.S., and Hasnain, S.S. (2011) Proton-coupled electron transfer in the catalytic cycle of *Alcaligenes xylosoxidans* copper-dependent nitrite reductase. *Biochemistry* **50**, 4121–4131
27. Kobayashi, K., Tagawa, S., Deligeer, and Suzuki, S. (1999) The pH-dependent changes of intramolecular electron transfer on copper-containing nitrite reductase. *J. Biochem.* **126**, 408–412
28. Wijma, H.J., Jeuken, L.J., Verbeet, M.P., Armstrong, F.A., and Canters, G.W. (2006) A random-sequential mechanism for nitrite binding and active site reduction in copper-containing nitrite reductase. *J. Biol. Chem.* **281**, 16340–16346
29. Wijma, H.J., Jeuken, L.J.C., Verbeet, M.P., Armstrong, F.A., and Canters, G.W. (2007) Protein film voltammetry of copper-containing nitrite reductase reveals reversible inactivation. *J. Am. Chem. Soc.* **129**, 8557–8565
30. Fukuda, Y., Tse, K.M., Kado, Y., Mizohata, E., Matsumura, H., and Inoue, T. (2015) Insights into unknown foreign ligand in copper nitrite reductase. *Biochem. Biophys. Res. Commun.* **464**, 622–628
31. Flot, D., Mairs, T., Giraud, T., Guijarro, M., Lesourd, M., Rey, V., van Brussel, D., Morawe, C., Borel, C., Hignette, O., Chavanne, J., Nurizzo, D., McSweeney, S., and Mitchell, E. (2010) The ID23-2 structural biology microfocus beamline at the ESRF. *J. Synch. Rad.* **17**, 107–118
32. Chapman, H.N., Fromme, P., Barty, A., White, T.A., Kirian, R.A., Aquila, A., Hunter, M.S., Schulz, J., DePonte, D.P., Weierstall, U., Doak, R.B., Maia, F.R., Martin, A.V., Schlichting, I., Lomb, L., Coppola, N., Shoeman, R.L., Epp, S.W., Hartmann, R., Rolles, D., Rudenko, A., Foucar, L., Kimmel, N., Weidenspointner, G., Holl, P., Liang, M., Barthelmess, M., Caleman, C., Boutet, S., Bogan, M.J., Krzywinski, J., Bostedt, C., Bajt, S., Gumprecht, L., Rudek, B., Erk, B., Schmidt, C., Homke, A., Reich, C., Pietschner, D., Struder, L., Hauser, G., Gorke, H., Ullrich, J., Herrmann, S., Schaller, G., Schopper, F., Soltau, H., Kuhnel, K.U., Messerschmidt, M., Bozek, J.D., Hau-Riege, S.P., Frank, M., Hampton, C.Y., Sierra, R.G., Starodub, D., Williams, G.J., Hajdu, J., Timneanu, N., Seibert, M.M., Andreasson, J., Rocker, A., Jonsson, O., Svenda, M., Stern, S., Nass, K., Andritschke, R., Schroter, C.D., Krasniqi, F., Bott, M., Schmidt, K.E., Wang, X., Grotjohann, I., Holton, J.M., Barends, T.R., Neutze, R., Marchesini, S., Fromme, R., Schorb, S., Rupp, D., Adolph, M., Gorkhover, T., Andersson, I., Hirsemann, H., Potdevin, G., Graafsma, H., Nilsson, B., and Spence, J.C. (2011) Femtosecond X-ray protein nanocrystallography. *Nature* **470**, 73–77
33. Kern, J., Alonso-Mori, R., Hellmich, J., Tran, R., Hattne, J., Laksmono, H., Glockner, C., Echols, N., Sierra, R.G., Sellberg, J., Lassalle-Kaiser, B., Gildea, R.J., Glatzel, P., Grosse-Kunstleve, R.W., Latimer, M.J., McQueen, T.A., DiFiore, D., Fry, A.R., Messerschmidt, M., Miahnahri, A., Schafer, D.W., Seibert, M.M., Sokaras, D., Weng, T.C., Zwart, P.H., White, W.E., Adams, P.D., Bogan, M.J., Boutet, S., Williams, G.J., Messinger, J., Sauter, N.K., Zouni, A., Bergmann, U., Yano, J., and Yachandra, V.K. (2012) Room temperature femtosecond X-ray diffraction of photosystem II microcrystals. *Proc. Natl. Acad. Sci. USA* **109**, 9721–9726
34. Johansson, L.C., Arnlund, D., Katona, G., White, T.A., Barty, A., DePonte, D.P., Shoeman, R.L., Wickstrand, C., Sharma, A., Williams, G.J., Aquila, A., Bogan, M.J., Caleman, C., Davidsson, J., Doak, R.B., Frank, M., Fromme, R., Galli, L., Grotjohann, I., Hunter, M.S., Kassemeyer, S., Kirian, R.A., Kupitz, C., Liang, M., Lomb, L., Malmerberg, E., Martin, A.V., Messerschmidt, M., Nass, K., Redecke, L., Seibert, M.M., Sjohamn, J., Steinbrener, J., Stellato, F., Wang, D., Wahlgren, W.Y., Weierstall, U., Westenhoff, S., Zatsepin, N.A., Boutet, S., Spence, J.C., Schlichting, I., Chapman, H.N., Fromme, P., and Neutze, R. (2013) Structure of a photosynthetic reaction centre determined by serial femtosecond crystallography. *Nat. Commun.* **4**, 2911
35. Kupitz, C., Basu, S., Grotjohann, I., Fromme, R., Zatsepin, N.A., Rendek, K.N., Hunter, M.S., Shoeman, R.L., White, T.A., Wang, D., James, D., Yang, J.H., Cobb, D.E., Reeder, B., Sierra, R.G., Liu, H., Barty, A., Aquila, A.L., Deponte, D., Kirian, R.A., Bari, S., Bergkamp, J.J., Beyerlein, K.R., Bogan, M.J., Caleman, C., Chao, T.C., Conrad, C.E., Davis, K.M., Fleckenstein, H., Galli, L., Hau-Riege, S.P., Kassemeyer, S., Laksmono, H., Liang, M., Lomb, L., Marchesini, S., Martin, A.V., Messerschmidt, M., Milathianaki, D., Nass, K., Ros, A., Roy-Chowdhury, S., Schmidt, K., Seibert, M., Steinbrener, J., Stellato, F., Yan, L., Yoon, C., Moore, T.A., Moore, A.L., Pushkar, Y., Williams, G.J., Boutet, S., Doak, R.B., Weierstall, U., Frank, M., Chapman, H.N., Spence, J.C., and Fromme, P. (2014) Serial time-resolved crystallography of photosystem II using a femtosecond X-ray laser. *Nature* **513**, 261–265
36. Kern, J., Alonso-Mori, R., Tran, R., Hattne, J., Gildea, R.J., Echols, N., Glöckner, C., Hellmich, J., Laksmono, H., Sierra, R.G., Lassalle-Kaiser, B., Koroidov, S., Lampe, A., Han, G., Gul, S., DiFiore, D., Milathianaki, D., Fry, A.R., Miahnahri, A., Schafer, D.W., Messerschmidt, M., Seibert, M.M., Koglin, J.E., Sokaras, D., Weng, T.-C., Sellberg, J., Latimer, M.J., Grosse-Kunstleve, R.W., Zwart, P.H., White, W.E., Glatzel, P., Adams, P.D., Bogan, M.J., Williams, G.J., Boutet, S., Messinger, J., Zouni, A., Sauter, N.K.,

Yachandra, V.K., Bergmann, U., and Yano, J. (2013) Simultaneous femtosecond X-ray spectroscopy and diffraction of photosystem II at room temperature. *Science* **340**, 491–495

37. Kern, J., Tran, R., Alonso-Mori, R., Koroidov, S., Echols, N., Hattne, J., Ibrahim, M., Gul, S., Laksmono, H., Sierra, R.G., Gildea, R.J., Han, G., Hellmich, J., Lassalle-Kaiser, B., Chatterjee, R., Brewster, A.S., Stan, C.A., Glockner, C., Lampe, A., DiFiore, D., Milathianaki, D., Fry, A.R., Seibert, M.M., Koglin, J.E., Gallo, E., Uhlig, J., Sokaras, D., Weng, T.C., Zwart, P.H., Skinner, D.E., Bogan, M.J., Messerschmidt, M., Glatzel, P., Williams, G.J., Boutet, S., Adams, P.D., Zouni, A., Messinger, J., Sauter, N.K., Bergmann, U., Yano, J., and Yachandra, V.K. (2014) Taking snapshots of photosynthetic water oxidation using femtosecond X-ray diffraction and spectroscopy. *Nat. Commun.* **5**, 4371
38. Hirata, K., Kawano, Y., Ueno, G., Hashimoto, K., Murakami, H., Hasegawa, K., Hikima, T., Kumasaka, T., and Yamamoto, M. (2013) Achievement of protein micro-crystallography at SPring-8 beamline BL32XU. *J. Phys. Conf. Ser.* **425**, 012002
39. Paithankar, K.S., and Garman, E.F. (2010) Know your dose: RADDOSE. *Acta Cryst. D* **66**, 381–388
40. Tanida, H., Kikuchi, A., Miura, K., Takeshita, K., Goto, S., Shiro, Y., and Ishikawa, T. (2004) XAFS and protein crystallography beamline BL38B1 at SPring-8. *AIP Conf. Proc.* **705**, 486–489
41. Fukuda, Y. and Inoue, T. (2015) High-temperature and high-resolution crystallography of thermostable copper nitrite reductase. *Chem. Commun.* **51**, 6532–6535
42. Otwinowski, Z. and Minor, W. (1997) Processing of X-ray diffraction data collected in oscillation mode. *Methods Enzymol.* **276**, 307–326
43. Vagin, A. and Teplyakov, A. (2010) Molecular replacement with MOLREP. *Acta Cryst. D* **66**, 22–25
44. Emsley, P., Lohkamp, B., Scott, W.G., and Cowtan, K. (2010) Features and development of Coot. *Acta Cryst. D* **66**, 486–501
45. Murshudov, G.N., Skubak, P., Lebedev, A.A., Pannu, N.S., Steiner, R.A., Nicholls, R.A., Winn, M.D., Long, F., and Vagin, A.A. (2011) REFMAC5 for the refinement of macromolecular crystal structures. *Acta Cryst. D* **67**, 355–367
46. Winn, M.D., Ballard, C.C., Cowtan, K.D., Dodson, E.J., Emsley, P., Evans, P.R., Keegan, R.M., Krissinel, E.B., Leslie, A.G., McCoy, A., McNicholas, S.J., Murshudov, G.N., Pannu, N.S., Potterton, E.A., Powell, H.R., Read, R.J., Vagin, A., and Wilson, K.S. (2011) Overview of the CCP4 suite and current developments. *Acta Cryst. D* **67**, 235–242
47. Chen, V.B., Arendall, W.B. III, Headd, J.J., Keedy, D.A., Immormino, R.M., Kapral, G.J., Murray, L.W., Richardson, J.S., and Richardson, D.C. (2010) MolProbity: all-atom structure validation for macromolecular crystallography. *Acta Crystallogr. D Biol. Crystallogr.* **66**, 12–21
48. Tono, K., Togashi, T., Inubushi, Y., Sato, T., Katayama, T., Ogawa, K., Ohashi, H., Kimura, H., Takahashi, S., Takeshita, K., Tomizawa, H., Goto, S., Ishikawa, T., and Yabashi, M. (2013) Beamline, experimental stations and photon beam diagnostics for the hard x-ray free electron laser of SACLA. *New J. Phys.* **15**, 083035
49. Son, S.-K., Chapman, H.N., and Santra, R. (2011) Multiwavelength anomalous diffraction at high X-ray intensity. *Phys. Rev. Lett.* **107**, 218102
50. Nass, K., Foucar, L., Barends, T.R., Hartmann, E., Botha, S., Shoeman, R.L., Doak, R.B., Alonso-Mori, R., Aquila, A., Bajt, S., Barty, A., Bean, R., Beyerlein, K.R., Bublitz, M., Drachmann, N., Gregersen, J., Jonsson, H.O., Kabsch, W., Kassemeyer, S., Koglin, J.E., Krumrey, M., Mattle, D., Messerschmidt, M., Nissen, P., Reinhard, L., Sitsel, O., Sokaras, D., Williams, G.J., Hau-Riege, S., Timneanu, N., Caleman, C., Chapman, H.N., Boutet, S., and Schlichting, I. (2015) Indications of radiation damage in ferredoxin microcrystals using high-intensity X-FEL beams. *J. Synch. Rad.* **22**, 225–238
51. Sugahara, M., Mizohata, E., Nango, E., Suzuki, M., Tanaka, T., Masuda, T., Tanaka, R., Shimamura, T., Tanaka, Y., Suno, C., Ihara, K., Pan, D., Kakinouchi, K., Sugiyama, S., Murata, M., Inoue, T., Tono, K., Song, C., Park, J., Kameshima, T., Hatsui, T., Joti, Y., Yabashi, M., and Iwata, S. (2014) Grease matrix as a versatile carrier of proteins for serial crystallography. *Nat. Methods* **12**, 61–63
52. Tono, K., Nango, E., Sugahara, M., Song, C., Park, J., Tanaka, T., Tanaka, R., Joti, Y., Kameshima, T., Ono, S., Hatsui, T., Mizohata, E., Suzuki, M., Shimamura, T., Tanaka, Y., Iwata, S., and Yabashi, M. (2015) Diverse application platform for hard X-ray diffraction in SACLA (DAPHNIS): application to serial protein crystallography using an X-ray free-electron laser. *J. Synch. Rad.* **22**, 532–537
53. Joti, Y., Kameshima, T., Yamaga, M., Sugimoto, T., Okada, K., Abe, T., Furukawa, Y., Ohata, T., Tanaka, R., Hatsui, T., and Yabashi, M. (2015) Data acquisition system for X-ray free-electron laser experiments at SACLA. *J. Synch. Rad.* **22**, 571–576
54. Yumoto, H., Mimura, H., Koyama, T., Matsuyama, S., Tono, K., Togashi, T., Inubushi, Y., Sato, T., Tanaka, T., Kimura, T., Yokoyama, H., Kim, J., Sano, Y., Hachisu, Y., Yabashi, M., Ohashi, H., Ohmori, H., Ishikawa, T., and Yamauchi, K. (2012) Focusing of X-ray free-electron laser pulses with reflective optics. *Nat. Photonics* **7**, 43–47
55. White, T.A., Kirian, R.A., Martin, A.V., Aquila, A., Nass, K., Barty, A., and Chapman, H.N. (2012) CrystFEL: a software suite for snapshot serial crystallography. *J. Appl. Cryst.* **45**, 335–341
56. Brehm, W. and Diederichs, K. (2014) Breaking the indexing ambiguity in serial crystallography. *Acta Cryst. D* **70**, 101–109
57. Karplus, P.A. and Diederichs, K. (2012) Linking crystallographic model and data quality. *Science* **336**, 1030–1033
58. Evans, P.R. and Murshudov, G.N. (2013) How good are my data and what is the resolution? *Acta Cryst. D* **69**, 1204–1214
59. Bublitz, M., Nass, K., Drachmann, N.D., Markvardsen, A.J., Gutmann, M.J., Barends, T.R.M., Mattle, D., Shoeman, R.L., Doak, R.B., Boutet, S., Messerschmidt, M., Seibert, M.M., Williams, G.J., Foucar, L., Reinhard, L., Sitsel, O., Gregersen, J.L., Clausen, J.D., Boesen, T., Gotfryd, K., Wang, K.-T., Olesen, C., Møller, J.V., Nissen, P., and Schlichting, I. (2015) Structural studies of P-type ATPase–ligand complexes using an X-ray free-electron laser. *IUCrJ* **2**, 409–420

60. Zhang, H., Boulanger, M.J., Mauk, A.G., Murphy, M.E.P. (2000) Carbon monoxide binding to copper-containing nitrite reductase from *Alcaligenes faecalis*. *J. Phys. Chem. B.* **104**, 10738–10742
61. Nakamura, K. and Go, N. (2005) Function and molecular evolution of multicopper blue proteins. *Cell. Mol. Life Sci.* **62**, 2050–2066
62. Lawton, T.J., Sayavedra-Soto, L.A., Arp, D.J., and Rosenzweig, A.C. (2009) Crystal structure of a two-domain multicopper oxidase: implications for the evolution of multicopper blue proteins. *J. Biol. Chem.* **284**, 10174–10180
63. Komori, H., Miyazaki, K., and Higuchi, Y. (2009) X-ray structure of a two-domain type laccase: a missing link in the evolution of multi-copper proteins. *FEBS Lett.* **583**, 1189–1195
64. MacPherson, I.S. and Murphy, M.E. (2007) Type-2 copper-containing enzymes. *Cell. Mol. Life Sci.* **64**, 2887–2899
65. Fraser, J.S., Clarkson, M.W., Degnan, S.C., Erion, R., Kern, D., and Alber, T. (2009) Hidden alternative structures of proline isomerase essential for catalysis. *Nature* **462**, 669–673
66. Fraser, J.S., van den Bedem, H., Samelson, A.J., Lang, P.T., Holton, J.M., Echols, N., and Alber, T. (2011) Accessing protein conformational ensembles using room-temperature X-ray crystallography. *Proc. Natl. Acad. Sci. USA* **108**, 16247–16252
67. Solomon, E.I., Szilagyi, R.K., DeBeer George, S., and Basumallick, L. (2004) Electronic structures of metal sites in proteins and models: contributions to function in blue copper proteins. *Chem. Rev.* **104**, 419–458
68. Murphy, M.E.P., Turley, S., and Adman, E.T. (1997) Structure of nitrite bound to copper-containing nitrite reductase from *Alcaligenes faecalis*. *J. Biol. Chem.* **272**, 28455–28460
69. Jacobson, F., Guo, H., Olesen, K., Okvist, M., Neutze, R., and Sjolin, L. (2005) Structures of the oxidized and reduced forms of nitrite reductase from *Rhodobacter sphaeroides* 2.4.3 at high pH: changes in the interactions of the type 2 copper. *Acta Cryst. D* **61**, 1190–1198
70. Lawton, T.J., Bowen, K.E., Sayavedra-Soto, L.A., Arp, D.J., and Rosenzweig, A.C. (2013) Characterization of a nitrite reductase involved in nitrifier denitrification. *J. Biol. Chem.* **288**, 25575–25583
71. Fukuda, Y., Tse, K.M., Lintuluoto, M., Fukunishi, Y., Mizohata, E., Matsumura, H., Takami, H., Nojiri, M., and Inoue, T. (2014) Structural insights into the function of a thermostable copper-containing nitrite reductase. *J. Biochem.* **155**, 123–135
72. Hough, M.A., Ellis, M.J., Antonyuk, S., Strange, R.W., Sawers, G., Eady, R.R., and Samar Hasnain, S. (2005) High resolution structural studies of mutants provide insights into catalysis and electron transfer processes in copper nitrite reductase. *J. Mol. Biol.* **350**, 300–309
73. Boulanger, M.J. and Murphy, M.E.P. (2002) Crystal structure of the soluble domain of the major anaerobically induced outer membrane protein (AniA) from pathogenic *Neisseria*: a new class of copper-containing nitrite reductases. *J. Mol. Biol.* **315**, 1111–1127
74. Desiraju, G.R. and Steiner, T. (1999) The Weak Hydrogen Bonds in Structural Chemistry and Biology Oxford University Press, Oxford
75. Antonyuk, S.V., Strange, R.W., Sawers, G., Eady, R.R., and Hasnain, S.S. (2005) Atomic resolution structures of resting-state, substrate- and product-complexed Cu-nitrite reductase provide insight into catalytic mechanism. *Proc. Natl. Acad. Sci.USA* **102**, 12041–12046